LA-UR-17-31103 (Accepted Manuscript)

Ignition and pusher adiabat

Cheng, Baolian
Kwan, Thomas J. T
Wang, Yi-Ming
Yi, Sunghwan
Batha, Steven H.

To be published in: Plasma Physics and Controlled Fusion

DOI to publisher's version: 10.1088/1361-6587/aac611

Permalink to record: http://permalink.lanl.gov/object/view?what=info:lanl-repo/lareport/LA-UR-17-31103

Ignition and pusher adiabat

Ignition and pusher adiabat

B. Cheng, T.J.T. Kwan, Y.M. Wang, S.A. Yi, S.H. Batha, and F. Wysocki*
Los Alamos National Laboratory, Los Alamos, New Mexico 87545, USA
(Dated: April 11, 2018)

In the last five years, large amounts of high quality data on inertial confinement fusion (ICF) experiments were produced at the National Ignition Facility (NIF). From this data we have significantly advanced our scientific understanding of the physics of thermonuclear (TN) ignition and identified critical issues that must be addressed to achieve a burning hotspot, such as implosion energetics, pusher adiabat, tamping effects, and confinement time. In this paper we present a review of recently developed TN ignition and implosion scaling theory [1, 2] that characterizes the thermodynamic properties of the hotspot and the ignition criteria for ICF. We compare our theoretical predictions with NIF data and find good agreement between theory and experiments. We demonstrate the fundamental effects of the pusher adiabat on the energy partition between the cold shell and the hot deuterium-tritium (DT) gas, and thus on the integrated performance of ICF capsules. Theoretical analysis of NIF experiments [3–5] and physical explanations of the discrepancies between theory, data, and simulations are presented. It is shown that the true experimental adiabat of the cold DT fuel can be inferred from neutron image data of a capsule implosion. We show that the ablator mix and preheat in the cold fuel can be estimated from the experimentally inferred hotspot mix. Finally, possible paths forward to reach higher yields at NIF implied by the theory are discussed.

PACS numbers: 83.10.Lk, 47.20.Ma, 83.20.Bg, 83.20.-d, 47.52.+j

INTRODUCTION

ICF experiments at NIF have made significant progress on improving neutron yields in the past several years. High-foot experiments at NIF have improved the capsule performance by more than an order of magnitude compared to the low-foot NIF ignition campaign (NIC) experiments through the high-foot drive profile that launched a higher pressure first shock than the low foot resulting in reduced ablation front instability and improved implosion quality [6, 7, 10–13]. Appreciable alpha-heating has been observed in a number of high-foot experiments [3, 7]. The recent high-density carbon shot N170827, driven by 1.78 MJ of laser energy, achieved a peak implosion velocity of 381 μm/ns, a hot-spot temperature of $\sim$4.8 keV, a neutron down scattering ratio (DSR) of $\sim$3.23 %, and the highest yield 1.78×10^{16} to date [14]. These experiments have certainly advanced NIF closer to ignition, yet predictive design methodologies for megajoule-yield ignition-class targets are still needed to support further progress. The NIC experiments also motivated significant modeling advances, such as in the understanding of the degradation in laser/target energy coupling due to parametric instabilities, improvements in computational models of non-local electron heat transport, etc.

In this invited paper we review advances in ignition theory that have progressed in parallel with the experimental achievements at NIF. We apply our theory to assess the performance of NIF integrated implosions and find that the current data trends are consistent with experimental adiabats that are higher than the intended design, particularly for targets that significantly underperformed relative to clean design simulations. Theoretical analysis of the experimental data is thus consistent with the observed trend that high adiabat target designs perform closer to predictions than those targets designed for a low adiabat. The underlying physical reasons for the difficulty of achieving "true" low adiabat implosions, as well as the practical implications on energetics requirements for high adiabat ignition schemes is a focus of this paper. Moreover, our theoretical work suggests practical future research directions for improving experimental yields on NIF, and these paths forward are the emphasis of our concluding section.

The article is specifically organized as follows, in section 2 and 3, we present the ignition criteria and its alternative forms. Section 4 outlines the implosion scaling and section 5 compares the theoretical predictions with experimental data. The pusher adiabat and mix are discussed in section 6. Finally section 7 summarizes the results and the paths forward.

IGNITION CRITERIA

In this section we recapitulate the ignition condition for ICF capsules [2], which imposes thresholds on the hotspot areal density and temperature below which ignition cannot occur. In particular we quantify how the thresholds are affected by loss mechanisms such as bremsstrahlung and electron thermal conduction.

Ignition occurs in the hotspot and is determined by the principle of energy balance, specifically by two time scales [1]: the fusion energy reproduction time ($\tau_{rep} = E_T/\dot{E}$) and the hydrodynamic disassembly time ($\tau_H =$

R_{hs}/C_s), where $E_T = 2\times(3/2)(n_D+n_T)kT+E_{rad}$ is the total energy density of the hot DT fuel, k is the Boltzmann constant, E_{rad} is the radiation energy density, and C_s is the adiabatic sound speed. The fusion energy deposition rate is $\dot{E} = n_T n_D \langle\sigma v\rangle_{DT} W_\alpha$, where W_α is the energy deposited into the hot DT per fusion reaction, which is normally given by a fraction f_α of the α-particle kinetic energy of 3.52 MeV [8, 9]. In this work, we choose $f_\alpha = 1$ for simplicity. We assume the neutron energy deposition is negligible because the mean free path of the 14 MeV neutrons is much larger than the hotspot radius R_{hs}. The energy loss due to collisions between α-particles and plasma electrons has been neglected because the α-particles are much heavier than the plasma electrons. To account for the tamping effect of the cold fuel, we replace the sound speed with an effective sound speed $C_s^* \equiv C_s/f_T$, where $f_T \propto \sqrt{\rho_p/\rho_{hs}}$ [3, 15, 16] is the tamping factor, and ρ_p and ρ_{hs} are the mass densities of the pusher and the hotspot at the interface between the hot and cold fuel, respectively. Here, we define the pusher as the sum of the remaining ablator and the cold DT.

In practice energy losses are inevitable, and the net energy deposition rate can be written as $\dot{E} = n_T n_D \langle\sigma v\rangle_{DT} W_\alpha - \sum_i dQ_l^i/dt$. Here the superscript i denotes various losses, such as the energy loss by electron bremsstrahlung, $dQ_l^b/dt = C_1\rho_{DT}^2 T^{1/2}$, and the heat loss by electron conduction, $dQ_l^e/dt = C_2 T^{3.35}/R_{hs}^2$ [17], where $C_1 \approx 9.1\times10^{22}$erg-cm^3/(keV$^{1/2}$g^{2}s), $C_2 \approx 6.9\times10^{19}$ erg/(keV$^{3.35}$cm-s), and T is in keV [2].

Ignition occurs when $\tau_{rep}/\tau_H \le 1$, the condition for self-sustained TN burn of the hotspot. This condition gives a threshold for the areal density of the hot DT

$$(\rho R)_{hs} \ge \frac{[(1+d)^2/d][3kT + E_{rad}/n_{DT}]C_s^* A_{DT}/N_A}{\langle\sigma v\rangle_{DT} W_\alpha - (\dot{Q}_l^b + \dot{Q}_l^e)(1+d)^2/(dn_{DT}^2)}, \quad (1)$$

where $n_{DT} \equiv n_D + n_T = \rho_{DT} N_A/A_{DT}$, $\dot{Q}_l^i \equiv dQ_l^i/dt$ $(i = b, e)$, $d = n_D/n_T$ is the D to T ratio, N_A is Avogadro's number, and A_{DT} is the atomic mass of the DT mixture. The nuclear reactivity $\langle\sigma v\rangle_{DT}$ [19] can be approximated by a power law of the temperature, T^n [2].

It is evident from Eq. (1) that any energy loss will increase the hotspot areal density required for ignition. Furthermore, the denominator being positive and definite, we make two important observations: (1) for $d = 1$, the energy loss by bremsstrahlung emission prevents ignition at temperatures below $T_{min} = \{[4C_1/(C_{DT}W_\alpha)](A_{DT}/N_A)^2\}^{2/7} \simeq 3$ keV at any $(\rho R)_{hs}$, and (2) the energy loss through electron heat conduction makes ignition impossible at any temperature when $(\rho R)_{hs} < \{[4C_2/(C_{DT}W_\alpha)](A_{DT}/N_A)^2 T^{-0.65}\}^{1/2} \simeq 0.13$ g/cm^2. These constraints may be improved if the burn is in equilibrium, i.e., when the bremsstrahlung and inverse-bremsstrahlung emission balance such that the associated energy loss is small relative to the heat capacity of the blackbody radiation losses.

For simplicity we now assume spherical symmetry with no mix, no energy loss from bremsstrahlung or electron heat conduction, and a blackbody radiation energy loss from the hot DT into the pusher. The effects of mix are analyzed in detail in a later section of this paper, while the effects of asymmetry will be treated in a future publication. Thus, Eq. (1) becomes

$$(\rho R)_{hs} \ge \frac{(1+d)^2}{d}\frac{[3kT + aT^4/n_{DT}]C_s^* A_{DT}}{\langle\sigma v\rangle_{DT} W_\alpha N_A}, \quad (2)$$

which gives ignition curves on the ρR-T plane under various conditions, as shown in Fig. 1. The general threshold depends on the ratio of D to T and has minimum at $d = 1$. Eq. (2) suggests two ways to achieve ignition: (1) low ρR at high temperature (i.e., NIF), or (2) high ρR at low temperature (i.e., stars). For example, the NIC ignition point design specifies $(\rho R)_{hs} \approx 0.3$ g/cm^2 and $T \approx 4$ keV [20]. Using the approximation $\langle\sigma v\rangle_{DT} \propto T^4$ and ignoring the radiation energy, Eq. (2) becomes

$$(\rho R)_{hs} \ge \frac{(1+d)^2}{d}\frac{\kappa_c}{f_T}\left(\frac{T}{\text{keV}}\right)^{-2.5} \text{g/cm}^2. \quad (3)$$

Here 3 keV $< T <$ 5.5 keV and $\kappa_c \equiv 12.683\times10^{-20}/C_{DT} \simeq 5.514$ is a constant that depends on the power law fit approximation for $\langle\sigma v\rangle_{DT}$. Eq. (3) represents an ideal lower limit for ignition at temperatures relevant to the NIC point design, while any departure from ideal conditions such as asymmetry, a decrease in α-particle energy deposition, or radiation and other energy losses would lead to higher threshold.

Fig. 1 shows various ignition curves at $f_T = 1$ on the ρR-T plane, showing that inclusion of the radiation heat capacity significantly raises the ignition threshold at temperatures above 3 keV. Below 3 keV, achieving ignition in an equilibrium mode is only feasible at high areal density. For reference we have also plotted in Fig. 1 the ignition curve including the effects of electron bremsstrahlung and heat conduction, which shifts the ignition space to higher temperatures (i.e., $T_{min} > 3.2$ keV).

ALTERNATIVE FORMS

In this section we explore the physical applications of our ignition criterion Eq. (2), including the minimum hotspot pressure and mass required for ignition and maximum hotspot that can be assembled given a fixed driver energy.

A. Lawson criterion. Substituting $\rho_{hs} = A_{DT}P/2RT$ (R is the gas constant) and $R_{hs} \approx C_s^*\tau_H$ into Eq. (3) gives the Lawson criterion [22]

$$P(\text{Gbar})\tau_H(\mu\text{s}) > \frac{2\kappa_c}{A_{DT}}\frac{(1+d)^2}{d}\frac{0.03472}{\gamma_g^{1/2}T(\text{keV})^2}. \quad (4)$$

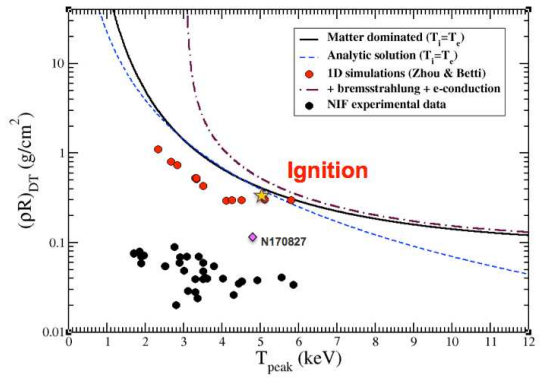

FIG. 1. **The ignition curve on the ρR-T plane for $f_T = 1$.** These curves characterize the ignition region under various assumptions regarding loss mechanisms.The black curve represents the ignition criterion in Eq. (2) when the radiation term is neglected. The maroon dot-dashed line includes the losses from both electron bremsstrahlung and heat conduction. The dashed blue curve is the analytic solution in Eq. (3) for the parameters of the NIC point design. The red dots denote the 1D numerical simulations performed by Betti et al. [21]. The black dots are experimental data from NIF including the NIC and high-foot campaigns. The golden star represents the goal of the NIC ignition target point design and the purple diamond is the record-yield shot to date.

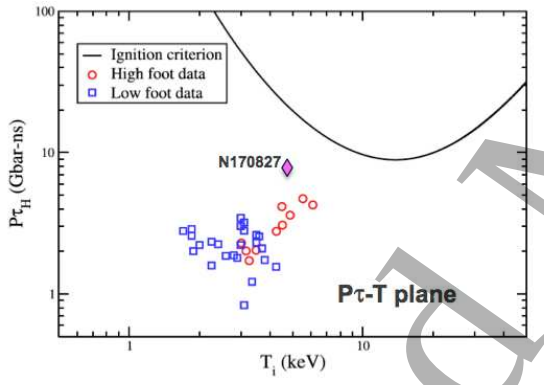

FIG. 2. Experimental data from NIF plotted against the ignition criterion in $P\tau_H - T$ space. The purple diamond represents the record performance high-density carbon shot N170827. In general, high-foot experiments show improved performance in $P\tau_H - T$ space relative to the low-foot NIC data.

Here we have used $C_s \equiv (2\gamma_g RT/A_{DT})^{1/2} \simeq 2.778 \times 10^7 \sqrt{\gamma_g T(\mathrm{keV})}$ cm/s. For $d = 1$ and $\gamma_g = 5/3$, substituting $\kappa_c = 5.514$ into the above equation gives $P(\mathrm{Gbar})\tau_H(\mu\mathrm{s}) \geq 0.475/T(\mathrm{keV})^2$. For example, at $T = 5.5$ keV and $R_{hs} \sim 30$ μm the required minimum hotspot pressure is ~ 375 Gbar, which is more stringent than the ignition conditions given in Ref. [23]. The pressure and confinement time achieved in selected NIF experiments is compared to the ignition criterion in Fig. 2. In the figure, we compare the experimental capsule performance in $P\tau_H - T$ space with respect to the ignition curve given by Eq. (2). Fig. 2 shows that even the record yielding high-density carbon shot N170827 is substantially below the ignition threshold. Thus, significant improvement in hotspot areal density or temperature, or both, is necessary to achieve ignition.

B. Minimum hotspot mass (M_{hs}) required for ignition. Sustaining TN burn and achieving ignition for a given hotspot temperature and target design (e.g., laser energy and convergence ratio) requires a minimum hot fuel mass. This minimum mass can be obtained from the ignition condition Eq. (3), and is related to the minimum energy required to assemble the hot core. For $T = 3$–5.5 keV the minimum mass is given by

$$M_{hs}^{min} \geq \frac{4\pi}{3}\frac{\kappa_c}{f_T}\frac{(1+d)^2}{T(\mathrm{keV})^{2.5}d}\frac{R_{0F}^2}{C_f^2}, \qquad (5)$$

where $C_f \equiv R_{0F}/R_{hs}$ is the geometric convergence ratio, and R_{0F} and R_{hs} are, respectively, the initial inner radius of the cold fuel and the final radius of the hotspot. For $d = 1$, $T = 4$ keV, $R_{0F} = 850$ μm, and $C_f \approx 35$, as in the NIC point design, the minimum hotspot mass is approximately 17 μg assuming $f_T = 1$. For $C_f \approx 27$, as in the high-foot design, the minimum hotspot mass is 29 μg if $f_T = 1$. Compared to the hotspot masses achieved in experiments, the minimum hotspot mass required for ignition is approximately four times greater. For example, M_{hs} was inferred as $\sim$3.9 μg in the low-foot shot N120321 [24] and $\sim$7.2 μg in the high-foot shot N130927 [7]. Our model thus implies that substantial improvements in the hotspot mass are required for ignition, which in turn necessitates greater energy delivery to the hot core.

We note that although the required minimum hotspot mass decreases dramatically at higher convergence ratios, the instabilities at the interface between the hot and cold fuel grow nonlinearly with C_f [50]. Thus, for high-convergence implosions it is a significant challenge to suppress the instabilities that mix cold fuel into the hotspot.

C. Maximum possible hotspot mass for a given driver energy. From the ideal ignition criterion given in Ref. [2] and the scaling laws in Ref. [1], we can estimate the maximum hotspot mass that can be achieved for a given driver energy. Let E_L^{max} be the maximum available laser energy and η_L be the ratio of pusher kinetic energy to the laser energy (i.e., the conversion efficiency from laser energy to pusher kinetic energy). Because not all kinetic energy is directed inward we have $M_p V_{imp}^2/2 \leq \eta_L E_L^{max}$, where V_{imp} is the peak implosion velocity in the radial direction and M_p is the mass of the pusher. The pusher and hotspot masses are related by the expression [1]

$$\frac{\eta}{2}M_p V_{imp}^2 = \frac{(3\gamma_p - 1)}{(\gamma_p - 1)}\epsilon_{hs} M_{hs}, \qquad (6)$$

where $\epsilon_{hs} = 2RT/[A_{DT}(\gamma_g - 1)]$ is the specific internal energy of the hotspot, η is the conversion efficiency from pusher kinetic energy to internal energy of the total stagnated mass, and γ_p and γ_g are, respectively, the adiabatic index of the pusher and hot DT gas. We thus obtain the maximum hotspot mass that can be assembled given a laser energy E_L^{max}

$$M_{hs}^{max} \leq \eta_L \eta \frac{(\gamma_p - 1)(\gamma_g - 1)}{(3\gamma_p - 1)} \frac{A_{DT} E_L^{max}}{2RT}. \quad (7)$$

Assuming a high adiabat implosion $\gamma_p = \gamma_g = 5/3$, $\eta_L \eta \approx 1.5\%$ (typical of NIF experiments), $E_L^{max} = 2$ MJ (the maximum NIF energy at 3ω), and $T = 5$ keV, we find $M_{hs}^{max} \leq 10$ μg. Thus, the maximum attainable hotspot mass for a high adiabat implosion given the available driver energy on NIF is less than the minimum hotspot mass required for ignition with the design parameters of the NIC or high-foot targets [2].

The maximum hotspot mass given $E_L^{max} = 2$ MJ can be improved if a low adiabat implosion can be achieved. As will be shown later in this paper, the data indicates that true low adiabat implosions are difficult to achieve in practice. On the other hand, in order to initiate ignition with the maximum hotspot mass $\sim$10 μg currently attainable on NIF, the hotspot convergence ratio must be greater than 40 [2]. As noted previously such a high convergence ratio poses a significant challenge due to the amplification of asymmetries and hydrodynamic instabilities. Thus, to achieve ignition at modest convergence ratios improvements must be made in (1) the maximum attainable hotspot mass through an increase in the coupling $\eta_L \eta$, or (2) the minimum required hotspot mass through an increase in the tamping factor f_T. Estimates of the increase in coupling or tamping needed to ignite without an improvement in E_L^{max} are given in Ref. [3].

IMPLOSION SCALING

In this section we summarize scaling laws that result from the least-energy implosion model given in Ref. [1]. The least-energy implosion model assumes that the total implosion kinetic energy is converted into the total internal energy of the capsule at stagnation time and then a pressure equilibrium between hot spot and pusher is achieved. Here, the pusher is the sum of the remaining ablator and the cold DT fuel, i.e., the total in-flight mass. The pusher plays two roles in the implosion energetics: (1) it is a carrier for the total kinetic energy available to do PdV work on the fuel and (2) it is a parasitic energy sink that absorbs some of the PdV work that would otherwise be done on the hot fuel. Thus, we applied the least-energy principle and minimized the pusher mass with respect to the hot spot pressure for a given peak implosion velocity. This leads to scaling laws that relate

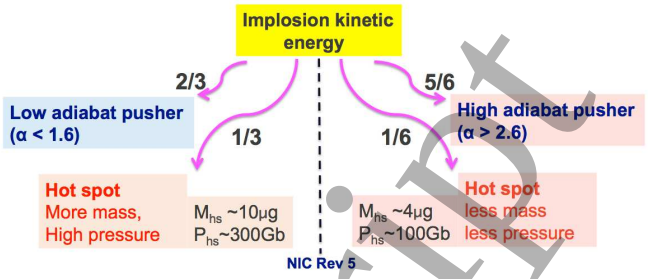

FIG. 3. Energy partition between pusher and hotspot for the low (left) and high (right) adiabat cases. Energy delivery to the hotspot is approximately halved if a true low adiabat implosion cannot be achieved. Here we take $\gamma_p = 3$ for the low adiabat case and $\gamma_p = 3/2$ for the high adiabat case in Eqs. (8), (12) and (14) to get these estimates.

the implosion and stagnation parameters. These scaling laws are useful in many cases, for example inferring the implosion adiabat from experimental observables or characterizing the energy partition between hotspot and pusher as a function of the adiabat.

Understanding of ignition thresholds requires a detailed accounting of the energy available in the implosion to assemble the required hotspot mass and surrounding cold fuel. For ICF implosions we can assume that the maximum implosion energy is attained at the peak velocity time and is equal to the pusher kinetic energy. The peak kinetic energy is thus the total energy budget available to heat the hotspot via pdV work during the stagnation phase.

Due to the finite available kinetic energy, the energy partition between the pusher and the hotspot during stagnation is an important factor in determining capsule performance. As discussed in previous work [3], the energy partition between pusher and hotspot is sensitive to the adiabat of the pusher. For a given peak kinetic energy, the hotspot internal energy can range from 1/6 of the total energy for a high adiabat to 1/3 of the total for a low adiabat. Since the hotspot mass is limited by the energetics, a high adiabat implosion that attains for example $M_{hs} \sim 3.5$ μg (at $\alpha \sim 3$) can achieve $M_{hs} \sim 10$ μg at a low adiabat $\alpha \sim 1.5$.

Fig. 3 illustrates how the energy partition between pusher and hot DT is affected by the adiabat of the pusher. A detailed optimum scaling relationship on mass, areal density, and size between the pusher and the hotspot at stagnation time is derived from the least energy implosion model [1] and given by the following expressions: the mass ratio

$$\frac{M_{hs}}{M_p} = \frac{(\gamma_p - 1)\eta V_{imp}^2}{(3\gamma_p - 1)2\epsilon_{hs}}, \quad (8)$$

the areal-density ratio

$$\frac{(\rho R)_{hs}}{(\rho R)_p} = \left[\left(1+\frac{2\gamma_p}{\gamma_g-1}\right)^{1/3} + \left(1+\frac{2\gamma_p}{\gamma_g-1}\right)^{2/3} + 1\right]\frac{M_{hs}}{M_p} \tag{9}$$

and

$$\frac{(\rho R)_{hs}}{(\rho R)_{tot}} = \frac{(\rho R)_{hs}/(\rho R)_p}{1+(\rho R)_{hs}/(\rho R)_p}, \tag{10}$$

the volume and aspect ratios

$$\frac{V_{hs}}{V_p} = \frac{\gamma_g-1}{2\gamma_p}, \quad \frac{\Delta_p}{R_{hs}} = \left[1+\frac{2\gamma_p}{\gamma_g-1}\right]^{1/3} - 1, \tag{11}$$

the energy ratio

$$\frac{E_{hs}}{E_p} = \frac{\gamma_p-1}{2\gamma_p}, \quad \frac{E_{hs}}{E_{tot}} = \frac{\gamma_p-1}{3\gamma_p-1}, \tag{12}$$

and the mass density ratio

$$\frac{\rho_{hs}}{\rho_p} = \frac{2\gamma_p}{(\gamma_g-1)}\frac{M_{hs}}{M_p} = [(1+\Delta_p/R_{hs})^3-1]\frac{M_{hs}}{M_p}. \tag{13}$$

Here, Δ_p is the thickness of the pusher at stagnation time. The subscripts "hs", "p" and "tot" represent hotspot, pusher and total, respectively. The hotspot pressure and neutron yield are given by the following scaling laws [2, 3]

$$\frac{P_{hs}}{P_0} = \left[\frac{\gamma_p}{(3\gamma_p-1)\epsilon_0}\eta_L\eta V_{imp}^2\right]^{\frac{\gamma_p}{\gamma_p-1}} \tag{14}$$

and

$$Y_n \approx 2.8\times10^6\,\frac{(\gamma_p-1)(\gamma_g-1)}{(3\gamma_p-1)}\left(\frac{M_p}{\mu g}\right)\left(\frac{V_{imp}}{\mathrm{km/s}}\right)^2\left(\frac{P_{hs}\tau_B}{\mathrm{Gb.ns}}\right)T^2, \tag{15}$$

where P_0, ρ_0, and ϵ_0 are, respectively, the pressure, mass density, and specific internal energy of the pusher at peak velocity time. Gb means Gigabar and τ_B is the burn width. Note that the burn width is the full width at half maximum of the neutron production rate. It is fundamentally different from the thermonuclear confinement time defined as the duration during which the fuel undergoes self-sustained TN burn [3]. We apply these scaling laws to the NIF data in the next section.

PREDICTIONS VS. EXPERIMENTS

In this section we compare the observed data trends to the theoretical scaling laws, and show how our theory can be applied to infer the true adiabat from the experimental data in the absence of direct measurements of the pusher entropy. We find that low adiabat implosions are difficult to achieve in practice, and that both the performance trends and neutron imaging data are consistent with high adiabat implosions.

Pressure vs. velocity scaling. Eq. (14) shows the dependence of the hotspot pressure on implosion velocity, adiabat, and the equation of state (EOS) of the pusher. For a low adiabat ($\gamma_p \simeq 3$) [3, 25], Eq. (14) recovers the scaling law $P_{hs} \propto V_{imp}^3$ extracted from ensemble code simulations [26]. For a high adiabat ($\gamma_p \simeq 5/3$), however, Eq. (14) gives $P_{hs} \propto V_{imp}^5$. This scaling is more consistent with the data trend $P_{hs} \propto V_{imp}^{4.73}$ observed in the high adiabat high-foot experiments by Hurricane et al. [27].

Figure 1 in Ref. [1] shows the above two scaling laws plotted against the low-foot NIC data. The agreement between the NIC data and the scaling $P_{hs} \propto V_{imp}^5$ indicates that both low- and high-foot implosions were in practice on a high adiabat [3] regardless the intended design adiabat.

It is worthwhile to point out that scaling law (14) has a general expression where the power law index is a function of the pusher adiabat. This is in contrast to the scaling law obtained in the simplest static isobaric model [29, 30] where the power law index is just a constant. For high adiabat ($\gamma_p = 5/3$), the scaling law (14) recovers the scaling law in the static isobaric model [31, 32] and for low adiabat ($\gamma_p = 3$), the scaling law (14) recovers the Livermore scaling law [33].

Yield vs. velocity scaling As shown in Eq. (15), the thermodynamic properties of the hotspot and the performance of the capsule uniquely depend on the peak implosion kinetic energy ($M_p V_{imp}^2/2$), the stagnation efficiency (η) and the adiabat of the pusher [1]. Incorporating the relation (14) between P_{hs} and V_{imp} into Eq. (15), together with the adiabatic heating scalings of perfect gas $R_{hs} \propto P_{hs}^{-1/3\gamma_g}$ and $T_{hs} \propto R_{hs}^{-3(\gamma_g-1)}$, and the scaling $\tau_B \propto R_{hs}/T^{1/2}$ assuming $\tau_B \propto \tau_H$, we obtain a power law dependence of the neutron yield on the peak implosion velocity [3],

$$Y_n \propto V_{imp}^{\Gamma} \quad \Gamma \equiv 2 + 2\frac{\gamma_p}{\gamma_p-1}\left(\frac{5}{2} - \frac{11}{6\gamma_g}\right).$$

Assuming $\gamma_g = 5/3$ for the hot DT gas, we obtain $\Gamma = 9$ in the case of a high adiabat ($\gamma_p = 5/3$), and $\Gamma = 6.2$ in the case of a low adiabat ($\gamma_p = 3$). The values of Γ and pusher adiabat α as a function of adiabatic index γ_p are plotted in Fig. 4. Where the pusher adiabat is defined as the mass averaged DT fuel pressure at a given density at peak implosion velocity time divided by the ideal Fermi degenerate pressure at the same density [3, 26].

In our theory the temperature of the hotspot scales with the peak implosion velocity as $T \propto V_{imp}^{2\gamma_p(\gamma_g-1)/[\gamma_g(\gamma_p-1)]}$. Thus, we predict that the higher the adiabat of the pusher, the more sensitive the hotspot temperature is to the peak implosion velocity. For high adiabat implosions in particular, small changes in the implosion velocity lead to large variations in the temperature of the hotspot and therefore the neutron yield.

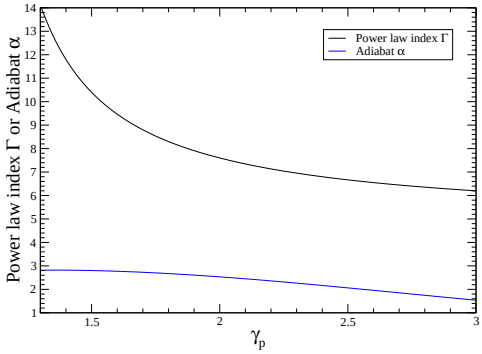

FIG. 4. The relationship between the adiabat α and adiabatic index γ_p of the pusher. Γ is the power law scaling index of the neutron yield to peak implosion velocity.

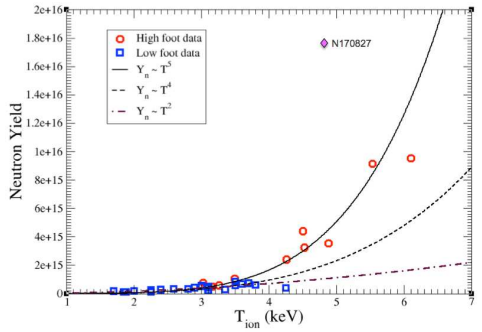

FIG. 5. Experimental data from the NIC and high-foot campaigns showing the scaling of neutron yield with hotspot temperature. The power law scaling index consistent with the data allows us to infer the experimentally achieved adiabat.

The relationship between implosion velocity, temperature, and yield has been thoroughly characterized in a large database of integrated NIF experiments [28]. Fig. 5 shows the observed dependence of the neutron yield to hotspot temperature, compared to theoretical predictions for different values of Γ (different adiabats). Because of $T_{hs} \propto V_{imp}^2$, we have $Y_n \propto T^5 \propto V_{imp}^{10}$. Thus the data is consistent with a power index of $\Gamma \approx 8-10$, which is in a good agreement with model predictions for the case of a high adiabat with $\gamma_p = \gamma_g = 5/3$ (Fig. 5 solid line).

Aspect ratio As shown in Eq. (11), the aspect ratio at stagnation Δ_p/R_{hs} is solely determined by the adiabat of the pusher. In NIF experiments, the radii of the hotspot and cold fuel can be measured from the primary and down-scattered neutron image data. The experimental uncertainties associated with the pusher thickness is usually larger than the uncertainties associated with the radius. In order to minimize the errors, we rewrite the aspect ratio as the ratio of the hotspot radius to the outer

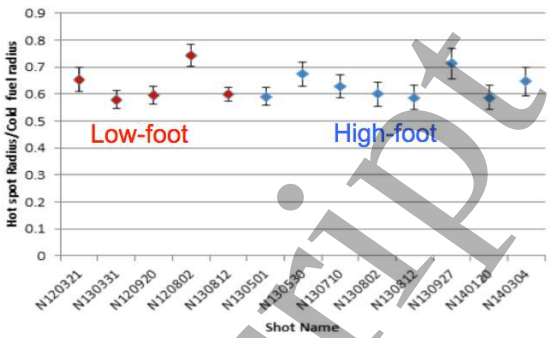

FIG. 6. Aspect ratio at stagnation, i.e., the ratio of the hotspot radius to the outer radius of the cold DT fuel (R_{hs}/R_{DT}), obtained from the neutron image data for both low- and high-foot experiments. Shot-to-shot fluctuations can be attributed to the slight variations of the adiabat due to differences in laser delivery, the thickness of the remaining ablator at different implosion velocities, and measurement uncertainties of the hotspot radius.

radius of the cold DT

$$\frac{R_{hs}}{R_{DT}} = \frac{1}{[1+2\gamma_p/(\gamma_g-1)]^{1/3}+\delta_a/R_{hs}}, \qquad (16)$$

where δ_a is the portion of the pusher thickness attributed to the remaining ablator. For $\gamma_g = 5/3$, and setting $\delta_a = 0$ for simplicity, Eq. (16) gives $R_{hs}/R_{DT} \approx 0.6$ if $\gamma_p = 5/3$ and $R_{hs}/R_{DT} \approx 0.465$ if $\gamma_p = 3$. These theoretical predictions can be directly compared with the neutron image data obtained in NIF experiments. We note that in reality $\delta_a \neq 0$, thus the measured aspect ratio should be slightly larger than the theoretical predictions.

Fig. 6 shows the aspect ratio R_{hs}/R_{DT} observed in both high-foot and low-foot experiments. Details of the neutron image data analysis are given in Refs. [34, 35]. The nearly constant value of 0.6 across the experimental data set agrees with our theoretical predictions for the high adiabat case, with $\gamma_g = 5/3$ and γ_p ranging from 4/3 to 5/3. This constant value indicates that in practice the adiabat was very similar in both the low- and high-foot experiments. Indeed, the data indicates that all of the shots were at a high adiabat state, regardless of the adiabat predicted by design code simulations. The significant difference in performance between the high- and low-foot designs is mainly caused by the unexpected large hydrodynamic instabilities and mix in the low-foot capsules. In the next section we explore the physical explanations for the high adiabat attained in practice in the laboratory.

We note in passing that using the measured aspect ratio together with Eq. (11), we may deduce the pusher adiabatic index γ_p as a function of the hot-spot adiabatic index γ_g and consequently the energy partition between the hotspot and the total fuel assembly as a function of the experimental aspect ratio and the fuel adiabatic

index according to Eq. (12) [1],

$$\frac{E_{hs}}{E_{tot}} = \frac{(\gamma_g - 1)[(1 + \Delta_p/R_{hs})^3 - 1]/2 - 1}{3(\gamma_g - 1)[(1 + \Delta_p/R_{hs})^3 - 1]/2 - 1}.$$

PUSHER ADIABAT AND MIX

In this section we recapitulate the results we obtained in Ref. [5] about how the presence of non-ideal effects such as preheat and 3D mix can modify the adiabat and we show how the theory can be applied to infer the fuel-ablator mix mass and preheat level consistent with the data-inferred adiabat, in the absence of direct measurements of the cold fuel mix.

As we have emphasized in earlier sections, the pusher adiabat strongly affects the hotspot pressure and capsule performance by determining the partition of energy, mass, and areal density between the hotspot and cold fuel at stagnation. Accurate implosion modeling thus depends on taking into account the perturbation that non-ideal and 3D effects have on the fuel specific entropy, since the adiabat is a measure of specific entropy. In particular, the change in specific entropy due to preheat, vorticity, and mix is given by [5]

$$\Delta s = \frac{\Delta Q}{M_{DT}T} + \frac{\nabla P}{nM_{DT}T} - \frac{N_{DT}k_B}{M_{DT}} \ln \frac{\chi^\chi}{(1+\chi)^{1+\chi}}, \quad (17)$$

where $\Delta Q \equiv C_v \Delta T$ is the fuel preheat and $\chi \equiv N_{CH}/N_{DT}$ is the mix concentration. Here, C_v is the specific heat for a fixed volume, n is the number density, and P the pressure of the cold fuel. N_{CH} and N_{DT} are, respectively, the number of molecules of CH mixed in the DT and the total number of DT molecules. The first term in Eq. (17) is the entropy change due to fuel preheat, the second term is the entropy change due to the vorticity from non-radial shear flow [36, 37], and the third term is the entropy change due to mixing from hydrodynamic instability growth. The adiabat change corresponding to such an entropy increase is given by the expression

$$\alpha = [1 + \exp(\frac{s_0 + \Delta s - 0.455}{0.063})]^{0.54}, \quad (18)$$

where $s_0 = 0.462$ GJ/g/keV is the specific entropy of the DT fuel at adiabat $\alpha = 1.5$ and temperature 26 K. Eq. (18) shows that the adiabat grows monotonically with entropy, so that any change in entropy due to non-ideal or 3D effects increases the adiabat of the DT fuel. We have shown in previous work [1–3, 5] that using a higher adiabat in a theoretical implosion model captures the performance degrading effects of hot electron preheat, vorticity and hydrodynamic instabilities.

The coupling between fuel adiabat and mix is clearly demonstrated in Eqs. (17,18). The adiabat α is increased when hydrodynamic instabilities lead to interpenetration and mixing of the ablator material and the cold fuel.

Clean mass fraction	0.87	0.7	0.0
Preheat (mJ)	30	0.0	0.0
Resulted adiabat	2.8	1.9	2.9
Design adiabat	1.5	1.5	1.5

TABLE I. The increase of pusher adiabat due to preheat and mix.

However, in many modern design simulations and theoretical ignition criteria the adiabat and mix are assumed to be decoupled. The adiabat increase due to hydrodynamic mix has been ignored in design simulations. For example, in the Ignition Threshold Factor (ITF) [6, 26] the term due to the effects of adiabat, $(\alpha/1.46)^{-4}$, and the term due to the fuel-ablator mix, $(M_{clean}/M_{DT})^{0.5}$, are independent and do not have cross-terms. Here, M_{clean} is the mass of the cold DT not contaminated by fuel-ablator mix. Such a decoupling assumption can underestimate the true implosion adiabat and thus overestimate the probability of ignition.

We now analyze NIF data to determine the adiabat increase produced in experiments due to mix. The total number of particles (both electrons and ions) is given by $N_{DT} = 2M_{DT}N_A/A_{DT}$, and for ignition capsule designs typical of the NIC and high-foot campaigns we have $M_{DT} \sim 170\mu$g. Setting $A_{DT} = 2.5$ we then have the number of particles $N_{DT} \sim 8.2 \times 10^{19}$. Assuming that vorticity is negligible, a clean fuel fraction of $M_{clean}/M_{DT} \sim 0.7$ (or $\chi \sim 0.215$) without any preheat gives from Eqs. (17,18) $\alpha \sim 1.9$, compared to a design adiabat of 1.5 for the NIC point design. In the case of complete mix ($N_{CH}/N_{DT} = 1$) the adiabat increase due to mix alone is sufficient to turn a low adiabat ($\alpha = 1.5$) design into a high adiabat ($\alpha = 2.9$) implosion. In the case where both preheat and mix are present even a moderate amount of these two effects leads to a substantial increase of the adiabat. For example, for a preheat of $\Delta Q \sim 30$ mJ and a relatively small mix ratio $N_{CH}/N_{DT} = 0.09$ (equivalent to 21.4 μg of CH penetrating the cold DT) the fuel winds up on a high adiabat ($\alpha = 2.8$). For clarity, we have summarized the effects of preheat and mix on the pusher adiabat in Table I.

The amount of preheat due to hot electrons, self-generated electric fields, and hard xrays has been estimated to range from 10 to 30 mJ [38]. In this case, 17 μg of CH mixed into the cold fuel is sufficient to place the implosion on a high adiabat, whereas 81 μg of fuel-ablator mix would be required to reach high adiabat if all preheat were eliminated. On the other hand, preheat levels above ∼40 mJ place the fuel on a high adiabat even if all fuel-ablator mix were to be suppressed. It is important to note that the ablator mass mixed into the cold fuel is significantly greater than the mass that mixes into the hotspot. Since only the mix into the hotspot is de-

tected through xray emission, there is currently no way to directly measure the precise mass of ablator material mixed into the cold fuel.

Consistent with the above examples, analysis in our previous works [3, 5] indicates that in practice very few NIF capsule implosions were on a low adiabat, contrary to design or postshot simulations [20]. Our analysis shows that most capsule implosions were on a high adiabat either due to mix and preheat, or by design due to the shock history of a high foot drive profile. The amount of CH mix mass and preheat consistent with the observed capsule performance can be inferred from experimental measurables, and are reported in Refs. [3, 5]. Inferring the mix mass from the data requires only the assumption that the mix mass is distributed uniformly in the cold DT. Such an assumption is consistent with detailed 2D and 3D postshot simulations [40] of NIC and high-foot experiments, as well as theoretical analysis of hydrodynamic instability growth and spike penetration of ablator material into the cold fuel [41].

Achieving a low adiabat ($\alpha \leq 1.6$), even in the absence of preheat and vorticity, requires suppression of the fuel-ablator mix to less than $N_{CH}/N_{DT} = 0.02$ [5]. This implies that the clean fuel fraction must be kept greater than $M_{clean}/M_{DT} = 1 - M_{CH}/M_{DT} = 0.972$. We emphasize that such a condition is much more restrictive than the rule of thumb typically adopted by capsule designers, $(M_{clean}/M_{DT})^{0.5} \geq 0.7$ [42]. Our calculations impose more stringent criteria for ignition target design, and suggest that designers must be more conservative in metrics such as the dopant concentration and the fraction of unablated mass at peak velocity. Moreover, such restrictive design criteria must be taken into account for planning future ICF facilities as they may lead to increased driver energy requirements.

Our analysis also highlights the need for accurate experimental diagnostics of the mass of ablator material mixed into the cold fuel, not just the central hotspot. Penetration of ablator material into the hotspot has been successfully measured in a number of NIC experiments [43, 44] and has also been inferred [45] from the enhanced xray self-emission and postshot simulations. Radiographic measurements of hydrodynamic instability growth at the fuel-ablator interface (seeded by preimposed perturbations) have also been reported [46]. Nonetheless, in an integrated ignition experiment there is currently no way to directly measure the mass of ablator material mixed into the cold DT.

When there is significant instability growth at the fuel-ablator interface, all of the spikes of ablator material penetrate through the cold DT and reach the hotspot. In other cases it is possible that a fraction of the ablator spikes reaches the hot core, while the rest only partially penetrate the cold fuel. Thus, we are likely to underestimate the mix mass inside the cold fuel when inferring the fuel-ablator mix from the emission enhancement due to hotspot mix. We can therefore make an estimate of the lower bound of the fuel-ablator mix from a measurement of the hotspot mix by assuming a uniform mix mass density in the hotspot and cold fuel regions. Under this assumption we can further estimate an upper bound for the cold fuel preheat by inferring the adiabat from the ratio of the hotspot radius to the cold fuel radius at stagnation.

Shot #	Adiabat	N_{CH}/N_{DT}	Mix in hotspot	Preheat
N120321	2.9	0.01	80 ng	< 40 mJ
N120405	2.9	0.98	> 4 μg	–
N120802	2.8	0.1	550 ng	< 30 mJ

TABLE II. Analysis of three low-foot NIC experiments with varying degrees of observed hotspot mix. In all NIC experiments the design adiabat was 1.5, in contrast with the high adiabats inferred from the data.

We now carry out such an estimate of the fuel-ablator mix mass for two representative experiments from the NIC campaign. NIF shot N120405 achieved a neutron yield 1.45×10^{14} and the hotspot mix inferred from the emission was $\sim$5.5 μg [45, 47], a significant fraction of the hotspot mass $\sim$9.5 μg [47]. Under the above assumptions, we estimate the mix between cold fuel and ablator as $N_{CH}/N_{DT} \sim 0.98$. Eqs. (17,18) then give an adiabat $\alpha \sim 2.85$ when preheat is assumed to be negligible, substantially higher than the design adiabat of 1.5 for the NIC point design. This increased adiabat is also consistent with the ratio of hotspot and cold fuel radii observed in the neutron images, $R_{hs}/R_{DT} \sim 0.7$ [3].

For our second example we analyze NIC shot N120802, which achieved a neutron yield 2.4×10^{14} and had an inferred hotspot mix mass $\sim$550 ng [45, 47] relative to a hotspot mass $\sim$5 μg [47]. We estimate that the fuel-ablator mix consistent with the observed hotspot mix is $N_{CH}/N_{DT} \sim 0.1$. Again, we use Eqs. (17,18) to arrive at a lower bound for the adiabat increase $\Delta\alpha \sim 0.21$ and $\alpha \sim 1.71$. In this case, however, the ratio of hotspot to shell radius $R_{hs}/R_{DT} \sim 0.75$ [3] implied by neutron imaging data is consistent with an adiabat of $\alpha \sim 2.8$. This discrepancy indicates that either (1) the observed hotspot mix underestimates the fuel-ablator mix because not all spikes that enter the cold fuel penetrate to the hot core, or (2) preheat is responsible for additional adiabat increase with an upper bound of 30 mJ or 0.17 J/kg. This example illustrates the need for a direct experimental diagnostic of fuel-ablator mix to break the degeneracy between the inferred mix and preheat consistent with the adiabat implied by neutron image data. We have summarized in Table II the adiabat, mix, and preheat consistent with the data for three representative NIC shots.

Similar to the trends observed in NIC, data from direct-drive implosions at OMEGA also indicate that hydro-instability induced mix led to significant perfor-

mance degradation in shots where the design adiabats were low ($\alpha < 2$) [48]. A similar analysis to the one presented above would conclude that the true adiabats in these mixed OMEGA shots were substantially higher than the clean design simulations due to the increase in adiabat from mix. Thus, an implosion model that takes into account the increased adiabat due to mix would result in better agreement with the observed performance.

It is worthwhile to point out that features of large implosion jets driven by the tent and fill tube in the low-foot implosion experiments are not included in the current analysis. These features not only affects the implosion symmetry and hot spot shape of the capsule but also increases the hot-spot mix and the pusher adiabat. The integral effects of the tent and fill tube cause further degradation in capsule performance. Recent NIF experiments demonstrated significant improvement in neutron yield by removing tent and reducing the size of fill tubes.

CONCLUSION AND PATHS FORWARD

In this section we present an analysis of the capsule energetics required for ignition, and conclude with possible research directions for improving the neutron yields on NIF. As we have discussed in the previous section, preheat and mix increase the effective adiabat of the cold fuel which leads to a less compressible pusher and results in reduced energy delivery to the hotspot during stagnation. On the other hand, ignition requires a minimum hotspot energy that can be derived from the minimum hotspot mass needed for propagating burn given by Eq. (5). For an ignition capsule with a hotspot of $T = 4$ keV, satisfying the ignition condition [2, 49] requires a hotspot mass of 26μg and a radius of 30μm. The minimum hotspot energy required for ignition is then $E_{hs} \simeq 2RTM_{hs}/[A_{DT}/(\gamma_g - 1)] \sim 12$kJ.

The total energy budget available for heating the hotspot via *pdV* work during stagnation can be estimated by the implosion kinetic energy at the time of peak velocity. The fraction of the energy budget delivered to the hotspot is given by the energy partition between hotspot and pusher, which is crucially sensitive to the pusher adiabat [1]. For a pusher where the remaining ablator is mass-matched to the DT, and where $M_{DT} \sim 170\mu$g for typical NIF ignition capsules, a peak implosion velocity of 370 km/s gives an implosion kinetic energy of $E_{imp} \sim 23$kJ. In particular, for the low adiabat ($\alpha \sim 1.5$) case $E_{imp}/3$ of the energy budget is delivered to the hotspot, versus $E_{imp}/6$ for the high adiabat ($\alpha \sim 3$) case. Therefore, if a low adiabat implosion can be achieved an implosion kinetic energy $E_{imp} \sim 36$kJ would suffice for ignition, whereas for the high adiabats that are currently achieved in practice an implosion kinetic energy $E_{imp} \sim 72$kJ is required. Thus a substantial increase in capsule scale size or velocity (or both) is required to meet the minimum implosion energy required for ignition. Detailed application to the required hydro scaling of NIF experiment will be given in a separate paper.

The laser drive energy required for ignition can be obtained from Eq. (7),

$$E_L \geq \frac{2RT(3\gamma_p - 1)}{A_{DT}\eta_L\eta(\gamma_p - 1)(\gamma_g - 1)} M_{hs}. \qquad (19)$$

For typical NIF experiments the overall coupling is given by $\eta_L\eta \approx 1\%$ and the minimum hotspot mass required for ignition is given by $M_{hs} = 26\mu$g at $T = 4$ keV. Thus, the minimum laser energy required for ignition is ~ 4.8 MJ if a low adiabat ($\gamma_p \sim 3$) can be achieved, and ~ 7.2 MJ for a high adiabat ($\gamma_p \sim 5/3$) implosion. It is important to note that mitigation of preheat and fuel-ablator mix is a necessary condition for achieving a true low adiabat, which in turn reduces the drive energy required for ignition.

Even for non-igniting capsules the neutron yield can be improved by increasing the hotspot energy, mass, and pressure using the currently available laser energy. Enhancing the performance of modern NIF targets thus requires improving the confinement metric $P_{hs}\tau_H$, given by

$$P_{hs}\tau_H = P_0 \left[\frac{\gamma_p}{(3\gamma_p - 1)\epsilon_0} \eta_L \eta V_{imp}^2 \right]^{\frac{\gamma_p}{\gamma_p - 1}} \tau_H. \qquad (20)$$

Eq. (20) identifies four possible paths forward for improving the performance of NIF targets: (1) Improving the available implosion kinetic energy by enhancing the drive coupling and optimizing the capsule design (ablator material, mass, and thickness); (2) Enhancing the ablation pressure and reducing the pusher adiabat by mitigating preheat and mixing and reducing the coasting time; (3) Lengthening the effective disassembly time by improving the implosion symmetry; and (4) Lengthening the effective disassembly time by increasing the inertial tamping through the use of dense high-Z liners on the inner surface of the ablator shell with a sharp metal-gas boundary. Recent successes on NIF demonstrating record yields with high-density carbon ablators and low coasting times show that increased capsule performance can indeed be achieved though the mitigation of mix in both the hotspot and cold fuel.

ACKNOWLEDGEMENTS

The authors wish to thank the referees for many valuable and constructive comments that led to notable improvement of our manuscript. The authors are grateful to P. Patel and C. Cerjan for sharing the NIC data, analysis, and calculations. We thank C. Cerjan, O.L. Landen, P. Amendt, D. Clark, H. Robey, B. Tipton and P. Bradley

for helpful discussions. We also acknowledge C.S. Carmer for editing this article. This work was performed under the auspices of the U.S. Department of Energy by the Los Alamos National Laboratory under Contract No. W-7405-ENG-36.

* bcheng@lanl.gov

* bcheng@lanl.gov

[1] B. Cheng, T. J. T. Kwan, Y.-M. Wang, and S. H. Batha, Phys. Rev. E 88, 041101 (2013).

[2] B. Cheng, T. J. T. Kwan, Y.-M. Wang, and S. H. Batha, Phys. Plasmas 21, 10270 (2014).

[3] B. Cheng, T. J. T. Kwan, Y. M. Wang, F. E. Merrill, C. J. Cerjan, and S. H. Batha, Phys. Plasmas 22, 082704 (2015).

[4] J. Melvin, H. Lim, V. Rana, B. Cheng, J. Glimm, D. H. Sharp and D. C. Wilson, Phys. Plasmas 22, 022708 (2015).

[5] B. Cheng, T. J. T. Kwan, Y. M. Wang, S. A. Yi, S. H. Batha, and F. J. Wysocki, Phys. Plasmas 23, 120702 (2016).

[6] J. D. Lindl, O. L. Landen, J. Edwards, E. I. Moses, J. Adams, P. A. Amendt, N. Antipa, P. A. Arnold, L. J. Atherton, S. Azevedo, D. Barker, M. A. Barrios, I. Bass, S. H. Baxamusa, R. Beeler, B. V. Beeman, P. M. Bell, L. R. Benedetti, L. Bernstein, L. Berzak Hopkins, S. D. Bhandarkar, T. Biesiada, R. M. Bionta, D. L. Bleuel, E. J. Bond, M. Borden, M. W. Bowers, D. K. Bradley, D. Browning, G. K. Brunton, J. Bude, S. C. Burkhart, R. F. Burr, B. Butlin, J. A. Caggiano, D. A. Callahan, A. C. Carpenter, C. W. Carr, D. T. Casey, C. Castro, J. Celeste, P. M. Celliers, C. J. Cerjan, J. Chang, M. Chiarappa-Zucca, C. Choate, T. J. Clancy, D. S. Clark, S. J. Cohen, G. W. Collins, A. Conder, J. R. Cox, P. S. Datte, G. A. Deis, E. L. Dewald, P. Di Nicola, J. M. Di Nicola, L. Divol, S. N. Dixit, T. Döppner, V. Draggoo, O. Drury, R. Dylla-Spears, E. G. Dzenitis, J. M. Dzenitis, M. J. Eckart, D. C. Eder, J. H. Eggert, R. B. Ehrlich, G. V. Erbert, J. Fair, D. R. Farley, M. Fedorov, B. Felker, R. Finucane, A. Fisher, D. N. Fittinghoff, J. Folta, R. J. Fortner, T. Frazier, G. Frieders, S. Frieders, S. Friedrich, J. Fry, J. Gaylord, S. M. Glenn, S. H. Glenzer, B. Golick, G. Gururangan, G. Guss, S. W. Haan, B. J. Haid, B. Hammel, A. V. Hamza, E. P. Hartouni, R. Hatarik, B. W. Hatch, S. P. Hatchett, R. Hawley, C. Haynam, J. Heebner, G. Heestand, M. R. Hermann, V. J. Hernandez, D. G. Hicks, D. E. Hinkel, D. D. Ho, J. P. Holder, D. Holunga, J. Honig, J. Horner, R. K. House, M. Hutton, N. Izumi, M. C. Jackson, K. S. Jancaitis, D. R. Jedlovec, M. A. Johnson, O. S. Jones, D. H. Kalantar, R. L. Kauffman, L. Kegelmeyer, G. Kerbel, M. Key, S. F. Khan, J. R. Kimbrough, R. Kirkwood, J. J. Klingman, J. A. Koch, T. R. Kohut, J. M. Koning, K. M. Knittel, B. J. Kozioziemski, G. W. Krauter, K. Krauter, A. Kritcher, J. Kroll, W. L. Kruer, G. LaCaille, K. N. LaFortune, L. J. Lagin, T. A. Land, A. B. Langdon, S. H. Langer, D. W. Larson, D. A. Latray, T. Laurence, S. LePape, R. A. Lerche, Z. Liao, J. Liebman, R. A. London, R. R. Lowe-Webb, T. Ma, B. J. MacGowan, A. J. MacKinnon, A. G. MacPhee, T. N. Malsbury, K. Manes, A. M. Manuel, E. R. Mapoles, M. M. Marinak, C. D. Marshall, D. Mason, N. Masters, D. G. Mathisen, I. Matthews, T. McCarville, J. M. McNaney, D. J. Meeker, N. B. Meezan, J. Menapace, P. Michel, P. E. Miller, J. L. Milovich, M. Mintz, R. Montesanti, M. Monticelli, J. D. Moody, M. J. Moran, J. C. Moreno, D. H. Munro, R. A. Negres, J. R. Nelson, M. Norton, M. Nostrand, M. O'Brien, Y. P. Opachich, C. Orth, A. E. Pak, E. S. Palma, J. N. E. Palmer, T. G. Parham, H.-S. Park, P. K. Patel, R. W. Patterson, J. E. Peterson, J. L. Peterson, T. Phillips, R. Prasad, K. Primdahl, S. T. Prisbrey, S. R. Qiu, J. E. Ralph, K. S. Raman, F. Ravizza, B. Raymond, B. A. Remington, M. A. Rever, J. Reynolds, M. J. Richardson, A. C. Riddle, B. Rittmann, M. D. Rosen, J. S. Ross, J. R. Rygg, R. A. Sacks, J. T. Salmon, J. D. Salmonson, J. D. Sater, R. L. Saunders, R. Sawicki, K. Schaffers, D. H. Schneider, M. B. Schneider, H. A. Scott, S. M. Sepke, R. Seugling, D. A. Shaughnessy, M. J. Shaw, R. Shelton, N. Shen, N. Shingleton, N. Simanovskaia, V. Smalyuk, D. A. Smauley, M. Spaeth, B. K. Spears, D. R. Speck, T. M. Spinka, P. T. Springer, M. Stadermann, W. Stoeffl, J. Stolken, C. Stolz, E. Storm, D. J. Strozzi, T. Suratwala, L. J. Suter, J. S. Taylor, C. A. Thomas, G. L. Tietbohl, R. Tommasini, D. Trummer, B. VanWonterghem, R. Von Rotz, R. J. Wallace, C. F. Walters, A. Wang, A. L. Warrick, S. Weaver, S. V. Weber, P. J. Wegner, K. Widmann, C. C. Widmayer, E. A. Williams, P. K. Whitman, K. Wilhelmsen, M. Witte, L. Wong, R. D. Wood, S. Yang, C. Yeamans, B. K. Young, B. Yoxall, R. A. Zacharias, G. B. Zimmerman, S. Batha, C. R. Danly, V. Fatherley, G. P. Grim, N. Guler, H. W. Herrmann, Y. Kim, J. L. Kline, G. A. Kyrala, R. J. Leeper, D. Martinson, F. E. Merrill, R. E. Olson, C. Wilde, M. D. Wilke, D. C. Wilson, G. A. Chandler, G. W. Cooper, K. D. Hahn, K. J. Peterson, C. L. Ruiz, K. C. Chen, N. Dorsano, M. Emerich, C. Gibson, D. Hoover, M. Hoppe, J. D. Kilkenny, K. Moreno, H. Wilkens, S. Woods, J. A. Frenje, M. G. Johnson, C. K. Li, R. D. Petrasso, H. Rinderknecht, M. Rosenberg, F. H. Sguin, A. Zylstra, W. Garbett, P. Graham, T. Guymer, A. S. Moore, J.-L. Bourgade, P. Gauthier, J.-P. Leidinger, L. Masse, F. Philippe and R. H. H. Scott Phys. Plasmas 21 , 129902 (2014).

[7] O. A. Hurricane, D. A. Callahan, D. T. Casey, P. M. Celliers, C. Cerjan, E. L. Dewald, T. R. Dittrich, T. Döppner, D. E. Hinkel, L. F. Berzak Hopkins, J. L. Kline, S. Le Pape, T. Ma, A. G. MacPhee, J. L. Milovich, A. Pak, H.- S. Park, P. K. Patel, B. A. Remington, J. D. Salmonson, P. T. Springer, and R. Tommasini, Nature 506, 343 (2014).

[8] G. S. Fraley, E. J. Linnebur, R. J. Mason, and R. L. Morse, Phys. Plasmas 17, 474, 1974.

[9] O. N. Krokhin and V. B. Rozanov, Sov. J. Quantum Electron. 2, 393 (1973).

[10] H.-S. Park, O. A. Hurricane, D. A. Callahan, D. T. Casey, E. L. Dewald, T. R. Dittrich, T. Döppner, D. E. Hinkel, L. F. Berzak Hopkins, S. Le Pape, T. Ma, P. K. Patel, B. A. Remington, H. F. Robey, J. D. Salmonson, and J. L. Kline, Phys. Rev. Lett. 112, 055001 (2014).

[11] J. Edwards, P. K. Patel, J. D. Lindl, L. J. Atherton, S. H. Glenzer, S. W. Haan, J. D. Kilkenny, O. L. Landen, E. I. Moses, A. Nikroo, R. Petrasso, T. C. Sangster, P. T. Springer, S. Batha, R. Benedetti, L. Bernstein, R. Betti, D. L. Bleuel, T. R. Boehly, D. K. Bradley, J. A. Caggiano, D. A. Callahan, P. M. Celliers, C. J. Cerjan, K. C. Chen, D. S. Clark, G. W. Collins, E. L. Dewald, L. Divol, S. Dixit, T. Doeppner, D. H. Edgell, J. E. Fair, M. Farrell, R. J. Fortner, J. Frenje, M. G. Gatu Johnson, E. Giraldez, V. Yu. Glebov, G. Grim, B. A. Hammel, A. V. Hamza, D. R. Harding, S. P. Hatchett, N. Hein, H. W. Herrmann, D. Hicks, D. E. Hinkel, M. Hoppe, W. W. Hsing, N. Izumi, B. Jacoby, O. S. Jones, D. Kalantar, R. Kauffman, J. L. Kline, J. P. Knauer, J. A. Koch, B. J. Kozioziemski, G. Kyrala, K. N. LaFortune, S. Le Pape, R. J. Leeper, R. Lerche, T. Ma, B. J. MacGowan, A. J. MacKinnon, A. Macphee, E. R. Mapoles, M. M. Marinak, M. Mauldin, P. W. McKenty, M. Meezan, P. A. Michel, J. Milovich, J. D. Moody, M. Moran, D. H. Munro, C. L. Olson, K. Opachich, A. E. Pak, T. Parham, H.-S. Park, J. E. Ralph, S. P. Regan, B. Remington, H. Rinderknecht, H. F. Robey, M. Rosen, S. Ross, J. D. Salmonson, J. Sater, D. H. Schneider, F. H. Sguin, S. M. Sepke, D. A. Shaughnessy, V. A. Smalyuk, B. K. Spears, C. Stoeckl, W. Stoeffl, L. Suter, C. A. Thomas, R. Tommasini, R. P. Town, S. V.Weber, P. J. Wegner, K. Widman, M. Wilke, D. C. Wilson, C. B. Yeamans, and A. Zylstra, Phys. Plasmas 20, 070501 (2013).

[12] D. S. Clark, D. E. Hinkel, D. C. Eder, O. S. Jones, S. W. Haan, B. A. Hammel, M. M. Marinak, J. L. Milovich, H. F. Robey, L. J. Suter, and R. P. J. Town, Phys. Plasmas 20, 056318 (2013).

[13] C. J. Cerjan, P. T. Springer, and S. M. Sepke, Phys. Plasmas 20, 056319 (2013).

[14] L. Berzak Hopkins , S. LePape , L. Divol , A. Pak , C. Goyon , E. Dewald , D. D. Ho , S. F. Khan , C. Weber , N. B. Meezan , J. Biener , G. Grim , T. Ma , J. L. Milovich , A. S. Moore , A. Nikroo , J. S. Ross , M. Stadermann , P. Volegov , C. Wild , D. A. Callahan , O. A. Hurricane , W. W. Hsing , R. P. J. Town , M. J. Edwards, Bulletin of the American Physical Society (59th Annual Meeting of the APS Division of Plasma Physics), Vol. 62, No. 12, 2017.

[15] S. Atzeni and J. Meyer-Ter-Vehn, The Physics of Inertial Fusion, Oxford, 2004.

[16] J. Nuckolls and Y.-L. Pan, Report No. UCRL-75876, Lawrence Livermore Laboratory, 1974.

[17] E. N. Avrorin, L. P. Feoktistov and L. I. Shibarshov, Sov. J. Plasma Phys., 6(5), 527, 1980.

[18] B. V. Litvinov, N. V. Ptitsyna, V. I. Chitaikin and L. I. Shibarshov, Physics-Doklady 336, 191 (1994).

[19] G. R. Caughlan and W. A. Fowler, Atomic data and nuclear data tables 40, 283-334 (1988).

[20] J. Edward, J. D. Lindl, B. K. Spears, S. V. Weber, L. J. Atherton, D. L. Bleuel, D. K. Bradley, D. A. Callahan, C. J. Cerjan, D Clark, G. W. Collins, J. E. Fair, R. J. Fortner, S. H. Glenzer, S. W. Haan, B. A. Hammel, A. V. Hamza, S. P. Hatchett, N. Izumi, B. Jacoby, O. S. Jones, J. A. Koch, B. J. Kozioziemski, O. L. Landen, R. Lerche, B. J. MacGowan, A. J. MacKinnon, E. R. Mapoles, M. M. Marinak, M. Moran, E. I. Moses, D. H. Munro, D. H. Schneider, S. M. Sepke, D. A. Shaughnessy, P. T. Springer, R. Tommasini, L. Bernstein, W. Stoeffl, R. Betti, T. R. Boehly, T. C. Sangster, V. Yu. Glebov, P. W. McKenty, S. P. Regan, D. H. Edgell, J. P. Knauer, C. Stoeckl, D. R. Harding, S. Batha, G. Grim, H. W. Herrmann, G. Kyrala, M. Wilke, D. C. Wilson, J. Frenje, R. Petrasso, K. Moreno, H. Huang, K. C. Chen, E. Giraldez, J. D. Kilkenny, M. Mauldin, N. Hein, M. Hoppe, A. Nikroo and R. J. Leeper, Phys. Plasmas 18, 051003 (2011).

[21] C. D. Zhou and R. Betti, Phys. Plasmas 15, 102707 (2008); Phys. Plasmas 14, 072703 (2007).

[22] J. D. Lawson, Proc. Phys. Soc. London, Sect. B 70, 6 (1957).

[23] R. Betti, P.Y. Chang,, B. K. Spears, K. S. Anderson, J. Edwards, M. Fatenejad, J. D. Lindl, R. L. McCrory, R. Nora1, and D. Shvarts, Phys. Plasmas 17, 058102 (2010).

[24] D. S. Clark, D.E. Hinkel, D. C. Eder, O. S. Jones, S. W. Haan, B. A. Hammel, M. M. Marinak, J. L. Milovich, H. F. Robey, L. J. Suter, and R. P. J. Town, Physics of Plasmas 20, 056318 (2013).

[25] Note that the code calculations did not actually use $\gamma_p = 3$, however, this analysis shows that the results from the code calculations are consistent with the results setting $\gamma_p = 3$ in this model.

[26] S. W. Haan, J. D. Lindl, D. A. Callahan, D. S. Clark, J. D. Salmonson, B. A. Hammel, L. J. Atherton, R. C. Cook, M. J. Edwards, S. Glenzer, A. V. Hamza, S. P. Hatchett, M. C. Herrmann, D. E. Hinkel, D. D. Ho, H. Huang, O. S. Jones, J. Kline, G. Kyrala, O. L. Landen, B. J. MacGowan, M. M. Marinak, D. D. Meyerhofer, J. L. Milovich, K. A. Moreno, E. I. Moses, D. H. Munro, A. Nikroo, R. E. Olson, K. Peterson, S. M. Pollaine, J. E. Ralph, H. F. Robey, B. K. Spears, P. T. Springer, L. J. Suter, C. A. Thomas, R. P. Town, R. Vesey, S. V. Weber, H. L. Wilkens, and D. C. Wilson, Phys. Plasmas 18, 051001 (2011).

[27] O.A. Hurricane, Bulletin of the American Physical Society, 57th Annual Meeting of the APS Division of Plasma Physics, 2015.

[28] D. Callahan, APS-DPP invited talk, 2014.

[29] J. Meyer-ter-Vehn, Nucl. Fusion 22, 561 (1982).

[30] M. Murakami and J. Meyer-ter-Vehn, Nucl. Fusion 31, 1315 (1991).

[31] M. M. Basko, Nucl. Fusion 38, 1779 (1998).

[32] M. M. Basko, Nucl. Fusion 35, 87 (1995).

[33] W. K. Levedahl and J. D. Lindl, Nucl. Fusion 37, 165 (1997).

[34] F.E. Merrill, D. Bower, R. Buckles, D.D. Clark, C.R. Danly, O.B. Drury, J.M. Dzenitis, V.E. Fatherley, D.N., Fittinghoff, R. Gallegos, and others, Rev. of Sci. Instrum. 83, 10D317 (2012).

[35] G. P. Grim, N. Guler, F. E. Merrill, G. L. Morgan, C. R. Danly, P. L. Volegov, C. H. Wilde, D. C. Wilson, D. S. Clark, D. E. Hinkel, O. S. Jones, K. S. Raman, N. Izumi, D. N. Fittinghoff, O. B. Drury, E. T. Alger, P. A. Arnold, R. C. Ashabranner, L. J. Atherton, M. A. Barrios, S. Batha, P. M. Bell, L. R. Benedetti, R. L. Berger, L. A. Bernstein, L. V. Berzins, R. Betti, S. D. Bhandarkar, R. M. Bionta, D. L. Bleuel, T. R. Boehly, E. J. Bond, M. W. Bowers, D. K. Bradley, G. K. Brunton, R. A. Buckles, S. C. Burkhart, R. F. Burr, J. A. Caggiano, D. A. Callahan, D. T. Casey, C. Castro, P. M. Celliers, C. J. Cerjan, G. A. Chandler, C. Choate, S. J. Cohen, G. W. Collins, G. W. Cooper, J. R. Cox, J. R. Cradick, P. S. Datte, E. L. Dewald, P. Di Nicola, J. M. Di Nicola, L. Divol, S. N. Dixit, R. Dylla-Spears, E. G. Dzenitis, M. J.

Eckart, D. C. Eder, D. H. Edgell, M. J. Edwards, J. H. Eggert, R. B. Ehrlich, G. V. Erbert, J. Fair, D. R. Farley, B. Felker, R. J. Fortner, J. A. Frenje, G. Frieders, S. Friedrich, M. Gatu-Johnson, C. R. Gibson, E. Giraldez, V. Y. Glebov, S. M. Glenn, S. H. Glenzer, G. Gururangan, S. W. Haan, K. D. Hahn, B. A. Hammel, A. V. Hamza, E. P. Hartouni, R. Hatarik, S. P. Hatchett, C. Haynam, M. R. Hermann, H. W. Herrmann, D. G. Hicks, J. P. Holder, D. M. Holunga, J. B. Horner, W. W. Hsing, H. Huang, M. C. Jackson, K. S. Jancaitis, D. H. Kalantar, R. L. Kauffman, M. I. Kauffman, S. F. Khan, J. D. Kilkenny, J. R. Kimbrough, R. Kirkwood, J. L. Kline, J. P. Knauer, K. M. Knittel, J. A. Koch, T. R. Kohut, B. J. Kozioziemski, K. Krauter, G. W. Krauter, A. L. Kritcher, J. Kroll, G. A. Kyrala, K. N. La Fortune, G. LaCaille, L. J. Lagin, T. A. Land, O. L. Landen, D. W. Larson, D. A. Latray, R. J. Leeper, T. L. Lewis, S. LePape, J. D. Lindl, R. R. Lowe-Webb, T. Ma, B. J. MacGowan, A. J. MacKinnon, A. G. MacPhee, R. M. Malone, T. N. Malsbury, E. Mapoles, C. D. Marshall, D. G. Mathisen, P. McKenty, J. M. McNaney, N. B. Meezan, P. Michel, J. L. Milovich, J. D. Moody, A. S. Moore, M. J. Moran, K. Moreno, E. I. Moses, D. H. Munro, B. R. Nathan, A. J. Nelson, A. Nikroo, R. E. Olson, C. Orth, A. E. Pak, E. S. Palma, T. G. Parham, P. K. Patel, R. W. Patterson, R. D. Petrasso, R. Prasad, J. E. Ralph, S. P. Regan, H. Rinderknecht, H. F. Robey, G. F. Ross, C. L. Ruiz, F. H. Sguin, J. D. Salmonson, T. C. Sangster, J. D. Sater, R. L. Saunders, M. B. Schneider, D. H. Schneider, M. J. Shaw, N. Simanovskaia, B. K. Spears, P. T. Springer, C. Stoeckl, W. Stoeffl, L. J. Suter, C. A. Thomas, R. Tommasini, R. P. Town, A. J. Traille, B. Van Wonterghem, R. J. Wallace, S. Weaver, S. V. Weber, P. J. Wegner, P. K. Whitman, K. Widmann, C. C. Widmayer, R. D. Wood, B. K. Young, R. A. Zacharias and A. Zylstra Phys. Plasmas 20, 056320 (2013).

[36] Z. Yoshida, ICTP Lecture at International Workshop on Cutting-Edge Plasma Physics, 2155-16, 2010.

[37] V. A. Thomas and R. J. Kares, Phys. Rev. Lett. 109, 075004 (2012).

[38] E. L. Dewald, F. Hartemann, P. Michel, J. Milovich, M. Hohenberger, A. Pak, O. L. Landen, L. Divol, H. F. Robey, O. A. Hurricane, T. Döppner, F. Albert, B. Bachmann, N. B. Meezan, A. J. MacKinnon, D. Callahan, and M. J. Edwards, Phys. Rev. Lett. 116, 075003 (2016).

[39] D. S. Clark, J. L. Milovich, D. E. Hinkel, J. D. Salmonson, J. L. Peterson, L. F. Berzak Hopkins, D. C. Eder, S. W. Haan, O. S. Jones, M. M. Marinak, H. F. Robey, V. A. Smalyuk, and C. R. Weber, Phys. Plasmas 21, 112705 (2014).

[40] D. Clark, APS Presentation, (2015).

[41] V. Rana, H. Lim, J. Melvin, and J. Glimm, B. Cheng and D. H. Sharp, submitted to Phys. Rev. E., 2016.

[42] B.A. Hammel, S.W. Haan, D.S. Clark, M.J. Edwards, S.H. Langer, M.M. Marinak, M.V. Patel, J.D. Salmonson, H.A. Scott' High Energy Density Physics 6, 171 (2010).

[43] S. P. Regan, R. Epstein, B. A. Hammel, L. J. Suter, J. Ralph, H. Scott, M. A. Barrios, D. K. Bradley, D. A. Callahan, C. Cerjan, G. W. Collins, S. N. Dixit, T. Doeppner, M. J. Edwards, D. R. Farley, S. Glenn, S. H. Glenzer, I. E. Golovkin, S. W. Haan, A. Hamza, D. G. Hicks, N. Izumi, J. D. Kilkenny, J. L. Kline, G. A. Kyrala, O. L. Landen, T. Ma, J. J. MacFarlane, R. C. Mancini, R. L. McCrory, N. B. Meezan, D. D. Meyerhofer, A. Nikroo, K. J. Peterson, T. C. Sangster, P. Springer and R. P. J. Town, Phys. Plasmas 19, 056307 (2012).

[44] S. P. Regan, R. Epstein, B. A. Hammel, L. J. Suter, J. Ralph, H. Scott, M. A. Barrios, D. K. Bradley, D. A. Callahan, C. Cerjan, G. W. Collins, S. N. Dixit, T. Doeppner, M. J. Edwards, D. R. Farley, S. Glenn, S. H. Glenzer, I. E. Golovkin, S. W. Haan, A. Hamza, D. G. Hicks, N. Izumi, J. D. Kilkenny, J. L. Kline, G. A. Kyrala, O. L. Landen, T. Ma, J. J. MacFarlane, R. C. Mancini, R. L. McCrory, N. B. Meezan, D. D. Meyerhofer, A. Nikroo, K. J. Peterson, T. C. Sangster, P. Springer and R. P. J. Town, Phys. Rev. Letts. 111, 045001 (2013). 85004 (2013).

[45] T. Ma, P. K. Patel, N. Izumi, P. T. Springer, M. H. Key, L. J. Atherton, L. R. Benedetti, D. K. Bradley, D. A. Callahan, P. M. Celliers, C. J. Cerjan, D. S. Clark, E. L. Dewald, S. N. Dixit, T. Döppner, D. H. Edgell, R. Epstein, S. Glenn, G. Grim, S. W. Haan, B. A. Hammel, D. Hicks, W. W. Hsing, O. S. Jones, S. F. Khan, J. D. Kilkenny, J. L. Kline, G. A. Kyrala, O. L. Landen, S. Le Pape, B. J. MacGowan, A. J. Mackinnon, A. G. MacPhee, N. B. Meezan, J. D. Moody, A. Pak, T. Parham, H.-S. Park, J. E. Ralph, S. P. Regan, B. A. Remington, H. F. Robey, J. S. Ross, B. K. Spears, V. Smalyuk, L. J. Suter, R. Tommasini, R. P. Town, S. V. Weber, J. D. Lindl, M. J. Edwards, S. H. Glenzer, and E. I. Moses, Phys. Rev. Lett. 111, 085004 (2013).

[46] C R Weber, T Döppner, D T Casey, T L Bunn, L C Carlson, R J Dylla-Spears, B J Kozioziemski, A G MacPhee, A Nikroo, H F Robey, J D Sater, V A Smalyuk, Phys. Rev. Lett. 117, 075002 (2016).

[47] P. Patel, NIF Presentation, October 8, 2013.

[48] T. C. Sangster, V. N. Goncharov, R. Betti, P. B. Radha, T. R. Boehly, D. T. Casey, T. J. B. Collins, R. S. Craxton, J. A. Delettrez, D. H. Edgell, R. Epstein, C. J. Forrest, J. A. Frenje, D. H. Froula, M. Gatu-Johnson, Y. Yu. Glebov, D. R. Harding, M. Hohenberger, S. X. Hu, I. V. Igumenshchev, R. Janezic, J. H. Kelly, T. J. Kessler, C. Kingsley, T. Z. Kosc, J. P. Knauer, S. J. Loucks, J. A. Marozas, F. J. Marshall, A. V. Maximov, R. L. McCrory, P. W. McKenty, D. D. Meyerhofer, D. T. Michel1, J. F. Myatt, R. D. Petrasso, S. P. Regan, W. Seka, W. T. Shmayda, R. W. Short, A. Shvydky, S. Skupsky, J. M. Soures, C. Stoeckl, W. Theobald, V. Versteeg, B. Yaakobi and J. D. Zuegel, Phys. Plasmas 20, 056317 (2013).

[49] R. Tipton, Private communications and preprint, "Generalized Lawson Criteria for Inertial Confinement Fusion", LLNL , 2015.

[50] K. Mikaelian, Phys. Rev. A 42, 4944 (1990).